Polymer Chemistry

PAPER

View Article Online
View Journal | View Issue

Cite this: *Polym. Chem.*, 2019, **10**, 4220

Cell-penetrating peptide modified AIE polymeric nanoparticles by miniemulsion polymerization and application for cell fluorescence imaging†

Yaxin Hu,[a] Xiaoqin Liang,[a] Zeyan Zhuang,[b] Zhihai Cao, *[a] Qi Qi,[a] Yijia Wang,[a] Yifang Mi,[a] Zujin Zhao*[b] and Qinmin Cui*[c]

Received 21st May 2019,
Accepted 27th June 2019

DOI: 10.1039/c9py00734b

rsc.li/polymers

Surface modification with bioactive groups is critical to the advanced bio-application of fluorescent nanoparticles (NPs), because it may offer specific interaction between the NPs and tissues, cells, as well as organelles. In this work, amino-functionalized aggregation-induced emission (AIE) polymeric NPs (AIE-PNPs) were efficiently synthesized through a one-pot miniemulsion copolymerization of methyl methacrylate and an amino-containing functional comonomer. The AIE-PNPs displayed a well-defined spherical morphology with a sub-100 nm particle size, and narrow particle size distribution. The surface of AIE-PNPs was further modified with maleimide groups and HIV-1 Tat peptides through a sequential carbodiimde reaction and a thiol-maleimide click reaction. The peptide-modified AIE-PNPs displayed good photostability and colloidal stability under continuous light irradiation or under various pH values, as well as good storage stability in aqueous media. The cell uptake efficiency of AIE-PNPs was significantly improved by the surface modification of HIV-1 Tat peptides, achieving good cell fluorescence imaging quality at a relatively low AIE-PNP concentration.

Introduction

Fluorescent nanoparticles (NPs) have drawn much attention due to their great potential application in photoelectric devices, probes, sensors, disease diagnosis and treatment, biological imaging, and bacterial detection and elimination.[1–6] In recent years, many fluorescent NPs have been devised and synthesized, including inorganic quantum dots, lanthanide-doped NPs, polymeric or inorganic NPs containing fluorescent dyes, and so forth.[7,8] As ideal fluorescent NPs for bio-applications, they should have suitable dimension and surface modification, high brightness, good photostability, low cytotoxicity, and more preferably, specific targeting ability.[9,10] Fluorescent polymeric NPs may be one of the most promising candidates for bio-applications, because they may meet the above-mentioned strict criteria for bio-applications through controlled synthesis and delicate surface modification.[7,11]

Traditionally, aggregation-caused quenching (ACQ) dyes are often used as functional components to build fluorescent NPs.[12] However, the ACQ dyes have the intrinsic low fluorescence quantum yield at high concentrations or under aggregated states, which somewhat limits their wide application.[13,14] In 2001, Tang *et al.* first reported a new type of fluorescent luminogens with unique aggregation-induced emission (AIE) property.[15,16] AIE luminogens (AIEgens) normally have a rotatable propeller-like structure and can emit strong fluorescence under the aggregated or confined state because of the restriction of intramolecular rotation.[13,14] The characteristics of AIEgens make them very suitable for preparing AIE polymeric NPs (AIE-PNPs).[11] On one hand, the confined environment inside the polymeric NPs is conducive to exciting the photoluminescence (PL) potential of AIEgens; on the other hand, the PL intensity of AIE-PNPs can be easily adjusted by the AIEgen content.[17]

Many innovative synthesis techniques have been designed to prepare AIE-PNPs with versatile colors and functionalities, including self-assembly of amphiphilic copolymers with

[a]*Key Laboratory of Advanced Textile Materials and Manufacturing Technology and Engineering Research Center for Eco-Dyeing & Finishing of Textiles, Ministry of Education, Zhejiang Sci-Tech University, Hangzhou 310018, China. E-mail: zhcao@zstu.edu.cn*
[b]*State Key Laboratory of Luminescent Materials and Devices, Center for Aggregation-Induced Emission, South China University of Technology, Guangzhou 510640, China. E-mail: mszjzhao@scut.edu.cn*
[c]*School of Pharmacy, Hangzhou Medical College, 481 Binwen Road, Hangzhou 310053, China. E-mail: cuiqm@hmc.edu.cn*

†Electronic supplementary information (ESI) available: Experimental, ^{1}H NMR spectra of TCF, TPE-CHO, and TPE-TCF, UV–vis spectra of peptide solution with known concentrations, standard curve of peptide, UV–vis spectrum of unreacted peptides, final conversions, particle sizes, and PDI values of miniemulsion polymerization systems with various AEMH contents, variables for calculation of surface amino density of NPs, and conductometric titration curves of NPs. See DOI: 10.1039/c9py00734b

AIEgens or AIEgen-containing amphiphilic copolymers induced by solvent evaporation,[18] supramolecular interaction,[19] or cross-linking,[20] flash nanoprecipitation,[21] aqueous dispersion polymerization,[22] emulsion polymerization,[23] miniemulsion polymerization,[17,24,25] and so on. The self-assembly-based technique can conveniently fabricate versatile AIE-PNPs, but in general, considering the controllability, most of the self-assembly processes have to be conducted at a low concentration, leading to a relatively poor fabrication efficiency. Emulsion polymerization or aqueous dispersion polymerization displays high feasibility to prepare various types of AIE-PNPs.[22,23] However, in emulsion polymerization systems, on one hand, latex particles are newly-produced through micellar nucleation and/or homogenous nucleation during the polymerization, and the latex particles are the main polymerization loci; on the other hand, monomers are mainly located in the monomer droplets of initial emulsion.[26] During the polymerization process, the monomers will diffuse from the monomer droplets to the nucleated latex particles as a result of monomer consumption in the nucleated latex particles.[26] In order to obtain AIE-PNPs, AIEgens that have been preloaded in the monomer droplets or aqueous continuous phase should diffuse to the nucleated latex particles. However, this diffusion is not a spontaneous process, and requires additional driving force. Therefore, for successfully preparing AIE-PNPs by emulsion polymerization, AIEgens should contain polymerizable groups, such as vinyl groups, to participate in the polymerization. Consequently, similar to the common monomers, the AIEgens with polymerizable groups can acquire driving force to diffuse to the nucleated latex particles to form AIE-PNPs.[23]

Miniemulsion polymerization technique has been proven as an efficient method to prepare polymeric, inorganic, and hybrid NPs.[27,28] In a typical miniemulsion system, many nanoscaled monomer droplets are homogenously dispersed in an aqueous continuous phase, and the latex particles are mainly formed through droplet nucleation.[26,29] Therefore, fluorescent PNPs can be conveniently prepared through miniemulsion polymerization by pre-loading fluorescent dyes in the monomer droplets.[30,31] However, in the early literature work, the loading amount of fluorescent dyes are often limited because of the notorious ACQ effect of the conventional dyes.[30] Recently, we first prepared AIE-PNPs through miniemulsion copolymerization of 1-allyl-1-methyl-2,3,4,5-tetraphenylsilole (AMTPS) and styrene (St).[17,25] Taking advantage of the AIE property of AMTPS, the loading amount of AMTPS could be as high as 20 wt% based on the overall monomer mass. More promisingly, the PL intensity of AIE-PNPs linearly increased with the increase of AMTPS content, indicating that the brightness of AIE-PNPs could be accurately tuned by the amount of AIEgens. The prepared AIE-PNPs through miniemulsion polymerization have been tentatively used for cell fluorescence imaging, displaying obvious merits of low cytotoxicity, high brightness, and good photostability.[25] More recently, thanks to the high colloidal stability of the miniemulsion polymerization system in a wide solid content range, we have prepared AIE-PNP emulsions with a solid content of up to 40 wt% through one-pot miniemulsion polymerization, significantly improving the preparation efficiency of AIE-PNPs.[24]

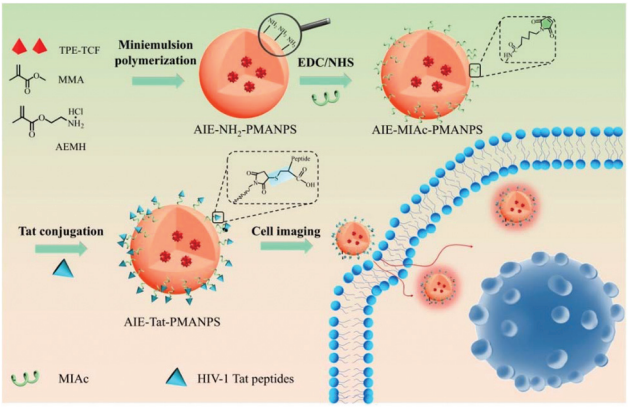

Scheme 1 Schematic representation of AIE-Tat-PMANPs synthesis and application for cell fluorescence imaging.

As a part of our series work, we focused on the delicate surface modification of AIE-PNPs in this work to further improve the application value of AIE-PNPs prepared by miniemulsion polymerization in biological fields, especially for cell fluorescence imaging. As shown in Scheme 1, amino-functionalized AIE-PNPs were efficiently prepared through one-pot miniemulsion copolymerization of amino-containing functional monomers (2-aminoethyl methacrylate hydrochloride, AEMH) and methyl methacrylate (MMA) by using 2-(3-cyano-5,5-dimethyl-4-(4-(1,2,2-triphenylvinyl)styry-l)furan-2(5*H*)ylid-ne) malononitrile (TPE-TCF) as the AIEgen. Subsequently, maleimide groups were introduced to the surface of AIE-PNPs through a carbodiimide reaction between the surface amino groups of AIE-PNPs and 6-maleimidocaproic acid (MIAc) with the help of *N*-(3-dimethylaminopropyl)-*N*′-ethylcarbodiimide hydrochloride (EDC) and *N*-hydroxysuccinimide (NHS). Finally, the maleimide groups served as the conjugation sites for cysteine (cys)-terminated HIV-1 Tat peptides *via* a thiol-maleimide click reaction. Compared with unmodified or amino-functionalized AIE-PNPs, AIE-PNPs modified with HIV-1 Tat peptides displayed much better cell uptake efficiency and cell image quality.

Experimental

Materials

MMA (AR, Tianjin Kermel Chemical Co., Ltd) was purified by reduced distillation, and then stored in a refrigerator prior to use. AEMH (90%, J&K Scientific), 2,2′-azodiisobutyronitrile (AIBN, 98%, Shanghai Aladdin Chemistry Co., Ltd), and hexadecane (HD, 99%, Acros Organics) were used as received. The non-ionic surfactant O-50, a poly(ethylene oxide)-hexadecyl ether with an ethylene oxide block length of ~50 units, was obtained from Jiangsu Hai'an Petrochemical Factory. EDC (98%), NHS (98%), and MIAc (98%) were obtained from

Shanghai Aladdin Chemistry Co., Ltd, and used as received. Cys-terminated HIV-1 Tat peptides (amino acid sequence, YGRKKRRQRRRC; molecular weight, 1663 g mol^{-1}; peptide purity, 97%) were synthesized by GenicBio Bioscience Co., Ltd. Bicinchoninic acid (BCA) protein assay kit was purchased from Beyotime Biotechnology. 4-Morpholine ethane sulfonic acid (MES, 99%) was obtained from Shanghai Aladdin Chemistry Co., Ltd. Dulbecco's modified essential medium (DMEM) and MTT solution were purchased from Thermo Fisher Scientific. Phosphate buffer saline (PBS) solution (0.01 M) was purchased from Beijing Leagene Biotech. Co., Ltd. Hydrochloric acid (HCl, AR, Hangzhou Shuanglin Chemistry Co., Ltd), sulfuric acid (H_2SO_4, AR, Shanghai Sanying Chemistry Co., Ltd), sodium hydroxide (NaOH, AR, Wuxi Zhangwang Chemistry Co., Ltd), potassium chloride (KCl, AR, Chengdu Dongjin Chemistry Co., Ltd), and potassium bromide (KBr, ACS, Shanghai Aladdin Chemistry Co., Ltd) were used as received. Deionized water was self-made and was used in all the experiments. Dimethyl sulfoxide-d6 (99.9%, 0.03% v/v tetramethyl silane) was purchased from Cambridge Isotope Laboratories, Inc. TPE-TCF was synthesized according to a reported method,[32] and the detailed synthetic route, description, and ^1H nuclear magnetic resonance (^1H NMR) spectra are presented in ESI (Scheme S1 and Fig. S1†).

Preparation of amino-functionalized AIE poly(MMA-*co*-AEMH) NPs through miniemulsion polymerization

Amino-functionalized AIE poly(MMA-*co*-AEMH) NPs (AIE-NH_2-PMANPs) were prepared through encapsulation of TPE-TCF *via* miniemulsion copolymerization of MMA and AEMH. The overall mass of MMA and AEMH was fixed at 1.0 g, and the weight content of AEMH varied in the range of 0–10 wt% relative to the overall amount of monomers. AIBN (0.02 g) and TPE-TCF (5.0 mg) was dissolved in the mixture of MMA and HD (0.06 g) to form a hydrophobic solution, which was used as the dispersed phase. AEMH and O-50 (0.2 g) were dissolved in water (12.5 g) to form an aqueous solution, which was used as the continuous phase. Secondly, two solutions were mixed and pre-emulsified under a magnetic agitation of 700 rpm at 40 °C for 15 min to obtain a crude emulsion. Subsequently, the crude emulsion was sonicated at 400 W for 9 min in an ice-water bath with a pulsed sequence (work 12 s, break 6 s) to obtain a stable monomer miniemulsion. After bubbled with nitrogen for 5 min, the monomer miniemulsion was sealed and reacted at 70 °C for 20 h with a magnetic agitation at 400 rpm to form an AIE-NH_2-PMANP emulsion. The as-synthesized AIE-NH_2-PMANP emulsion was purified by dialysis against deionized water for 3 days (the cutoff molecular weight (MWCO) of dialysis membrane was 5000 g mol^{-1}). The AIE-NH_2-PMANPs with various AEMH contents were named as AIE-*X*% NH_2-PMANPs, in which *X*% represents the weight content of AEMH.

For comparison, the AIE PMMA NPs without amino-functionalization were synthesized through miniemulsion polymerization of MMA (1.0 g). The preparation protocol was the same as that of the AIE-NH_2-PMANP emulsions.

Surface modification of AIE-10%NH_2-PMANPs with HIV Tat peptides

The surface maleimide modification of AIE-10%NH_2-PMANPs was conducted through a carbodiimide reaction with the help of EDC and NHS.[33] Briefly, MIAc (40 mg) was dissolved in 10 g MES buffer (pH = 6.0), followed by adding EDC (50 mg) and NHS (30 mg). The reactants were activated at 25 °C for 60 min. The AIE-10%NH_2-PMANP emulsion (8 g, 2.6 wt%) was diluted with 10 g PBS solution, and then the activated solution was added. Subsequently, the pH value of the reaction medium was adjusted to 7.2 ± 0.2 by 0.1 M aqueous NaOH solution. After 12 h reaction, the resulted maleimide-modified AIE polymeric NPs (AIE-MIAc-PMANPs) were dialyzed against deionized water for 3 days to remove the unreacted EDC, NHS, and MIAc.

Cys-terminated HIV-1 Tat peptides (500 μg) were dissolved in 0.5 mL deionized water, and the aqueous solution was mixed with 5 mL of AIE-MIAc-PMANP emulsion (0.5 wt%). The mixture was uniformly mixed and reacted at 25 °C for 12 h to prepare peptide-modified AIE polymeric NPs (AIE-Tat-PMANPs). The obtained product was purified by dialysis against deionized water for 3 days.

Determination of surface amino density of AIE-NH_2-PMANPs

Surface amino density of AIE-NH_2-PMANPs was determined by conductometric back titration.[24] Briefly, 2 g of the dialyzed emulsion was diluted with 70 g deionized water, and the pH value of diluted emulsions was adjusted to 10.5 ± 0.2 by aqueous NaOH solution (0.1 mol L^{-1}). The titration was started after the conductivity reached a stable value. 10 μL of aqueous H_2SO_4 solution (0.13 mol L^{-1}) was added into the emulsion in one shot every one minute, and the equilibrated conductivities were recorded. The conductometric back titration was finished until the pH value of emulsion decreased to 3.5 ± 0.2.

The molar amount of amino groups per gram of AIE-NH_2-PMANPs (S_b, μmol g^{-1}) was calculated through eqn (1):

$$S_b = S'_b - S_0 \quad (1)$$

where S'_b (μmol g^{-1}) is the molar amount of amino groups per gram of AIE-NH_2-PMANPs directly calculated through eqn (2); the emulsion of AIE PMMA NPs was used as the blank sample, and S_0 is the calculated molar amount of hypothetical surface amino groups per gram of AIE PMMA NPs through eqn (3).

$$S'_b = \frac{V_b \times C \times 2}{W \times m} \times 10^{-6} \quad (2)$$

$$S_0 = \frac{V_0 \times C \times 2}{W_0 \times m_0} \times 10^{-6} \quad (3)$$

where V_b is the volume of H_2SO_4 consumed by OH^- ions ionized by the amino groups of NPs and H_2O (μL), V_0 is the volume of H_2SO_4 consumed by the AIE PMMA NPs, C is the concentration of aqueous H_2SO_4 solution (mol L^{-1}), m and m_0 are the masses of emulsion used for conductometric back titration (g), and W and W_0 are the solid contents of dialyzed emulsions (wt%).

The molar amount of amino groups per square meter was calculated through eqn (4):

$$[\mu\text{mol m}^{-2}] = S_b \times \frac{\rho \times D_n \times 10^{-6}}{6} \quad (4)$$

where ρ is the density of copolymer (1.18×10^6 g L^{-1}), and D_n is the number-average particle size of the NPs.

BCA assay for quantification of surface coupled HIV-1 Tat peptides

A calibration curve of HIV-1 Tat peptide solution with known concentrations was made on the basis of the standard BCA assay protocol (Fig. S2A and S2B†). The unreacted HIV-1 Tat peptides were collected through centrifugation of NP emulsions with a concentrator (M_w = 10 000 g mol^{-1}) to collect the solution. The solid samples were obtained through freeze-drying, and then were re-dissolved in 1 mL water to obtain an aqueous solution of peptides. After processed through the standard BCA assay protocol, the absorbance at 562 nm of the aqueous solution of peptides was measured on a UV-2600 UV–vis spectrometer (Shimadzu Corporation). The peptide concentration was calculated through fitting the measured value in the standard curve. The amount of surface coupled HIV-1 Tat peptides was calculated through material balance.

Evaluation of photostability and colloidal stability of AIE-Tat-PMANPs

AIE-Tat-PMANPs and TPE-TCF nanoaggregates formed in the THF/water mixture with a water fraction of 90% in volume were exposed to continuous irradiation by a 460 nm light for 3600 s on a Hitachi F-4600 spectrofluorometer. The PL intensity at 590 nm was monitored to evaluate the photostability of the AIE-Tat-PMANPs and TPE-TCF nanoaggregates.

Photostability and colloidal stability of AIE-Tat-PMANPs and TPE-TCF nanoaggregates at various pH conditions were evaluated as follows: emulsions of AIE-Tat-PMANPs and TPE-TCF nanoaggregates were diluted with water at various pH values (pH = 2–11). The particle sizes of AIE-Tat-PMANPs and TPE-TCF nanoaggregates at various pH values were determined by dynamic light scattering (DLS). The PL spectra of AIE-Tat-PMANPs and TPE-TCF nanoaggregates in the spectral range of 480–750 nm under various pH conditions were collected at an excitation wavelength of 460 nm.

The storage stability was evaluated as follows: the particle sizes of AIE-Tat-PMANPs were measured by DLS, and PL spectra in the range of 480–750 nm were collected at an excitation wavelength of 460 nm every 2 days, respectively.

MTT assay for evaluation of cytotoxicity of AIE-PNPs

HeLa cells were seeded at a density of 1×10^5 cells per mL in 96-well plates, and incubated for 24 h at 37 °C. Subsequently, the emulsions of AIE PMMA NPs, AIE-10%NH_2-PMANPs, and AIE-Tat-PMANPs with various NP concentrations were added to the dispersion of cells, and co-incubated for another 24 h. The sample and control wells were washed twice with PBS solution, and then the freshly prepared MTT solution (0.5 mg mL^{-1}, 100 μL) was added. After 4 h incubation at 37 °C, the MTT solution was removed and washed twice with PBS solution. DMSO (100 μL) was then added to each well and the plate was gently shaken at room temperature for 10 min to dissolve all formed precipitates. The absorbance of the sample and control wells at 570 nm was then measured by a microplate reader. Cell viability was calculated by the ratio of the absorbance of the sample to the control cells.

Fluorescence cell imaging and mean signal intensity

The emulsions of AIE PMMA NPs, AIE-10%NH_2-PMANPs, and AIE-Tat-PMANPs (4 μL, 1 mg mL^{-1}) were dispersed in 1 mL of DMEM culture medium, respectively, following co-incubation with HeLa cells of 2.5×10^5 cells per mL for different time lengths (4, 6, and 12 h) at 37 °C. Subsequently, the culture medium was removed and the cells were washed with PBS solution for three times. The cells mounted onto a rectangular glass slide, followed by fluorescence imaging using a Zeiss LSM7 DUO laser scanning confocal microscope (Germany; excitation at 488 nm; emission filter: 420–720 nm). The mean signal intensity of the fluorescence image was analyzed by ZEN (Blue) software.

Characterization

Z-Average particle sizes and polydispersibility (PDI) values of the NPs were measured by DLS (Zetasizer Nanoseries) at 25 °C under a scattering angle of 90°. Prior to measurement, a drop of emulsion was diluted with 2 mL water. Particle sizes were given as the average of three measurements. Particle morphologies were characterized by a JSM-1200EX transmission electron microscope operated at 80 kV. The preparation of TEM samples was as follows: a drop of emulsion was diluted with 20 mL water; a drop of the diluted sample was placed on a 400-mesh carbon-coated copper grid and dried at 40 °C for 20 h. Zeta potential values of AIE PMMA NPs, AIE-NH_2-PMANPs, AIE-MIAc-PMANPs, and AIE-Tat-PMANPs were measured at 25 °C by using a Zetasizer nanoseries potentiometer. Prior to measurements, AIE PMMA NP and AIE-NH_2-PMANP emulsions were diluted to a solid content of 0.25 wt% with aqueous KCl solution at various pH values (10^{-3} mol L^{-1}, pH = 2–11), respectively; AIE-MIAc-PMANP and AIE-Tat-PMANP emulsions were diluted to a solid content of 0.25 wt% with aqueous KCL solution (10^{-3} mol L^{-1}, pH = 7.0 ± 0.2), respectively. PL spectra of the diluted aqueous emulsions of AIE-NH_2-PMANPs with various AEMH contents and AIE-Tat-PMANPs (20 μL in 2 mL water) were recorded on a Hitachi F-4600 spectrofluorometer in a spectral range of 480 to 750 nm at the excitation wavelength of 460 nm. Chemical structure of AIE-10% NH_2-PMANPs and AIE-MIAc-MANPs were determined by ^{1}H NMR spectroscopy on a Bruker AV 400 NMR spectrometer using DMSO-d6 as the solvent and tetramethylsilane as the internal standard. Fourier transform infrared (FTIR) spectra of AIE-10%NH_2-PMANPs and AIE-MIAc-PMANPs were recorded in transmission mode on a Vertex 70 FTIR spectrometer (Bruker Optics, Germany).

Results and discussion

Synthesis and particle properties of AIE-NH_2-PMANPs

AIE-NH_2-PMANPs were prepared through miniemulsion copolymerization of MMA and AEMH by using TPE-TCF as the AIEgen. The weight content of AEMH relative to the overall monomers was varied from 0 to 10 wt%. The final conversions of miniemulsion polymerization systems with various AEMH contents were about 90% (Fig. S3†). The *Z*-average particle sizes and PDI values of AIE-NH_2-PMANPs with various AEMH contents were characterized by DLS, and the results are shown in Fig. 1A. In the range of 0–10 wt% of AEMH, the particle sizes of AIE-NH_2-PMANPs were slightly influenced by the AEMH content, and they varied in the size range of 89–97 nm. Further increase of the AEMH content led to an obvious increase of particle size and PDI value (Fig. S4†). A typical TEM image of the AIE-10%NH_2-PMANPs is shown in Fig. 1B. The AIE-10%NH_2-PMANPs displayed a well-defined spherical morphology and a narrow particle size distribution. The number-average particle size of this sample determined by TEM was 79.9 ± 8.4 nm. The small particle size and the relatively narrow particle size distribution of AIE-10%NH_2-PMANPs are beneficial to the further biological applications, like cell fluorescence imaging.

The amino densities of the AIE-NH_2-PMANPs with various AEMH contents were determined by the conductometric back titration. The detailed data for calculation of surface amino density are given in Fig. S5 and Table S1.† The results showed that the amino density of AIE-NH_2-PMANPs exhibited a positive correlation with the AEMH content (Fig. 2A). The amino density of AIE-10%NH_2-PMANPs was 9.18 μmol m^{-2}.

The isoelectric points (IEPs) of AIE-NH_2-PMANPs with various AEMH contents were measured by zeta potential measurements, and the results are shown in Fig. 2B. With the increase of AEMH content from 0 to 2.5 wt%, the IEPs of AIE-NH_2-PMANPs drastically increased from 3.1 to 9.5. When the AEMH content was higher than 2.5 wt%, the IEPs of AIE-NH_2-PMANPs slightly increased with the increase of AEMH content in the pH range of 9.5–10.5. This result is consistent with the reported IEPs of amino-functionalized polymeric particles.[34] The relatively high IEPs of AIE-NH_2-PMANPs with more than 2.5 wt% of AMEH confirmed the successful surface amino-functionalization of the AIE-NH_2-PMANPs.

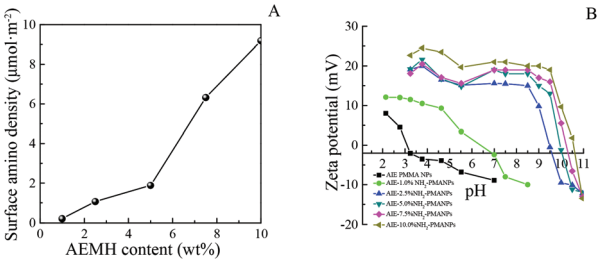

Fig. 2 (A) Surface amino densities of AIE-NH_2-PMANPs with various AEMH contents. (B) Zeta potential values of AIE-NH_2-PMANPs with various AEMH contents at various pH values.

PL properties of AIE-NH_2-PMANPs

In the AIE-NH_2-PMANPs, the TPE-TCF molecules were embedded in the poly(MMA-*co*-AEMH) matrix, and thus they could emit bright orange-red fluorescence due to the restriction of intramolecular rotation of TPE-TCF (Fig. 3A inset). Quantitatively, a strong PL peak in the spectral range of 480–750 nm appeared in the PL spectra of AIE-NH_2-PMANPs, regardless of the AEMH content (Fig. 3A). As a molecule with a donor–acceptor structure, the PL behavior of TPE-TCF is affected by environmental polarity.[32] Generally speaking, with the increase of environmental polarity, the emission wavelength of TPE-TCF will be red-shifted and the PL intensity will decrease due to the twisted intramolecular charge transfer (TICT) effect. However, the AEMH content did not show any obvious effect on the maximum emission wavelength of the AIE-NH_2-PMANPs, and all the PL spectra centered at ~590 nm (Fig. 3A). This may be due to the fact that the TPE-TCF molecules were in a confined state and condensed in the AIE-NH_2-PMANPs, and thus the majority of TPE-TCF molecules (inner molecules) felt less change of polymer polarity and barely experienced TICT effect.

It is interesting to find that compared with the AIE PMMA NPs, the PL intensity of AIE-NH_2-PMANPs was enhanced with addition of AEMH monomer (Fig. 3B). With introduction of AEMH units to the copolymer chains, the interaction between the polymer chains was enhanced, leading to the reduced mobility of chain segments. In other words, the TPE-TCF molecules were embedded in a more closely-packed polymer

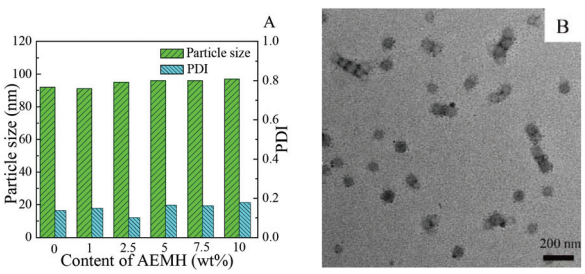

Fig. 1 (A) Particle sizes and PDI values of AIE-NH_2-PMANPs with various AEMH contents. (B) Typical TEM image of the AIE-10%NH_2-PMANPs.

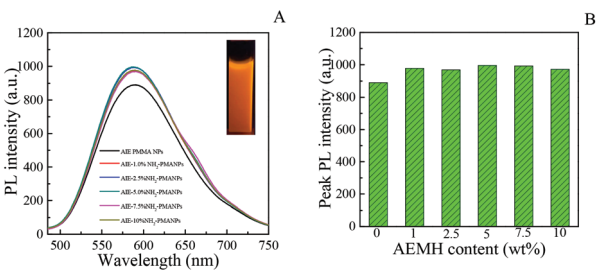

Fig. 3 PL spectra (A) and peak PL intensities (B) of AIE-NH_2-PMANPs with various AEMH contents. (A inset, photo of AIE-10%NH_2-MANP emulsion under UV light irradiation).

matrix, and thus the intramolecular rotation of TPE-TCF became more restricted, which resulted in the increased PL intensity of AIE-NH_2-PMANPs.

Surface modification of AIE-10%NH_2-PMANPs with HIV-1 Tat peptides

As presented in the previous section, the AIE-10%NH_2-PMANPs emitted bright orange-red fluorescence. Moreover, the AIE-10%NH_2-PMANPs displayed a well-defined spherical structure, and their particle size was less than 100 nm. More importantly, the AIE-10%NH_2-PMANPs had plenty of surface amino groups for further sophisticated modification with bioactive groups. Therefore, the AIE-10%NH_2-PMANPs were chosen as the typical AIE PNPs for the further peptide modification and cell imaging experiments. It has been reported that the HIV-1 Tat peptide could significantly promote the uptake efficiency of NPs by cells.[35–37] Therefore, in this work, the HIV-1 Tat peptide was chosen as the representative peptide to modify the AIE-10%NH_2-PMANPs. AIE-Tat-PMANPs were synthesized through a carbodiimide reaction and a thiol/maleimide click reaction in sequence.

Firstly, the maleimide groups were introduced to the surface of AIE-10%NH_2-PMANPs through the carbodiimide reaction with the assistance of EDC and NHS by using as MIAc as the coupling agent. As shown in Fig. 4A, compared with the spectrum of the AIE-10%NH_2-PMANPs (curve a, Fig. 4A), new peaks at 1651 and 1540 cm^{-1} appeared in the spectrum of AIE-MIAc-PMANPs (curve b, Fig. 4A), which could be assigned to the amide I band (stretching vibration of C=O) and the amide II band (plane bending vibration of N–H), respectively.[38] The ^1H NMR spectra of AIE-10%NH_2-PMANPs and AIE-MIAc-PMANPs are shown in Fig. 4B. Compared with the AIE-10%NH_2-PMANPs (curve a, Fig. 4B), the appearance of a new peak at 7.0 ppm (curve b, Fig. 4B) indicates the presence of maleimide group in the AIE-MIAc-PMANPs.[39]

In order to further confirm the attachment of maleimide groups to the AIE-10%NH_2-PMANPs, the surface charge of AIE-MIAc-PMANPs was measured to compare with that of the AIE-10%NH_2-PMANPs, and the results are shown in Fig. 4C. The zeta potential of AIE-MIAc-PMANPs was 4.0 mV at pH 7.0, much lower than that of the AIE-10%NH_2-PMANPs (21.0 mV) at the same pH value. The reduced surface charge of AIE-MIAc-PMANPs could be reasonably ascribed to the partial replacement of amino groups with maleimide groups.

In summary, the FTIR, ^1H NMR, and zeta-potential results came to a conclusion that the AIE-10%NH_2-PMANPs had been successfully surface-modified with the maleimide groups to form AIE-MIAc-PMANPs.

Furthermore, AIE-Tat-PMANPs were synthesized through a thiol–ene click reaction between the maleimide groups of AIE-MIAc-PMANPs and sulfydryl groups of cys-ended HIV-1 Tat peptides. The IEP of HIV-1 Tat peptides is about 12.5, and the zeta potential is 8.0 mV at pH 7.0.[40] As a result of attachment of positively charged HIV-1 Tat peptides, the zeta potential of AIE-Tat-PMANPs increased to 14.0 mV at pH 7.0 (Fig. 4C). According to the BCA assay result (Fig. S2C†), about 103 μg of HIV-1 Tat peptides were attached to the surface of NPs, giving a surface coupling density of 2.39 μmol g^{-1}.

Photostability and colloidal stability of AIE-Tat-PMANPs

Photostability and colloidal stability of fluorescent NPs are critical to their biological application.[41,42] Therefore, the photostability of AIE-Tat-PMANPs and TPE-TCF nanoaggregates was evaluated by continuous irradiation of 460 nm light for 1 h, and the results are shown in Fig. 5A. The PL intensity of AIE-Tat-PMANPs slightly decreased at the beginning of irradiation, and remained almost constant after 300 s irradiation. The final loss of the PL intensity was ~5.2% after 1 h irradiation, displaying a good photostability against continuous irradiation. In comparison, the TPE-TCF nanoaggre-

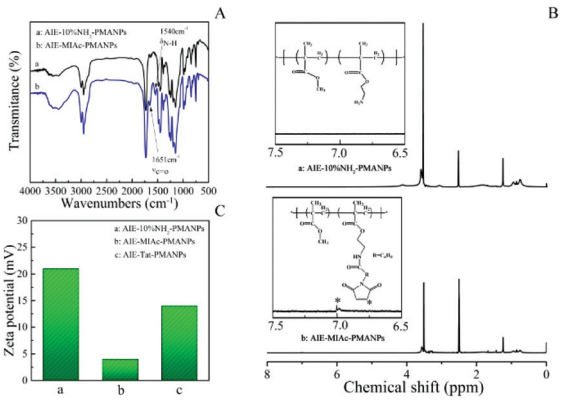

Fig. 4 FTIR (A) and ^1H NMR (B) spectra of AIE-10%NH_2-PMANPs and AIE-MIAc-PMANPs. Zeta potential values of AIE-10%NH_2-PMANPs, AIE-MIAc-PMANPs, and AIE-Tat-PMANPs at pH 7.0 (C).

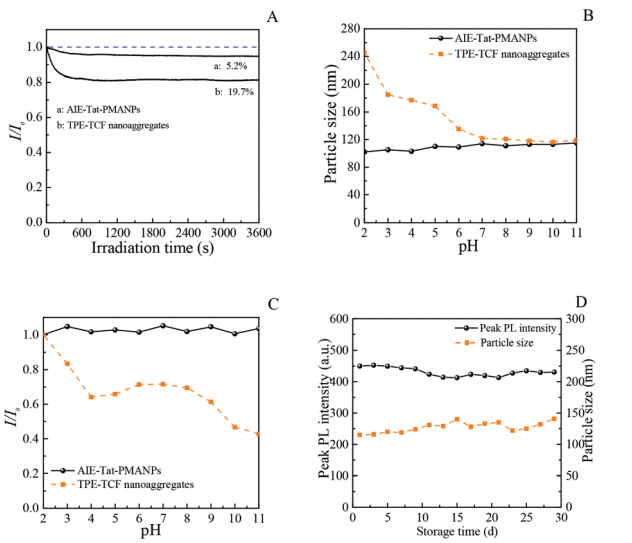

Fig. 5 Normalized PL intensity of the AIE-Tat-PMANPs and TPE-TCF nanoaggregates during continuous irradiation of 460 nm light for 1 h (A). Particle sizes (B) and normalized peak PL intensity (C) of the AIE-Tat-PMANPs and TPE-TCF nanoaggregates under various pH values. PL intensity and particle sizes of the AIE-Tat-PMANPs during storage (D).

gates in a THF/water mixed solvent underwent a more serious PL loss (~19.7%) under the same irradiation condition. All the results indicated that the AIE-Tat-PMANPs exhibited a better photostability, compared with the TPE-TCF nanoaggregates, thanks to encapsulation of TPE-TCF molecules by the polymer matrix.

Normally, the pH environment in normal cells is neutral, while the physiological environment in cancer cells is acidic.[9] Moreover, the pH environment of extracellular compartments and intracellular organelles is often different, such as endosomes and lysosomes (pH ≈ 5.0), and extracellular tumor tissues (pH ≈ 6.5).[9,43] Therefore, the photostability and colloidal stability of AIE-Tat-PMANPs and TPE-TCF nanoaggregates at various pH values was also evaluated. In comparison with the significant variation of particle size of TPE-TCF nanoaggregates, the particle size of AIE-Tat-PMANPs only slightly increased with the increase of pH values, exhibiting a good colloidal stability (Fig. 5B). As shown in Fig. 5C, the PL intensity of TPE-TCF nanoaggregates significantly depended on the pH values of medium. It obviously decreased with the increase of the pH values of media. On the contrary, the AIE-Tat-PMANPs displayed an excellent photostability against the pH variation. This could be reasonably ascribed to the isolation of the embedded TPE-TCF molecules from the exterior environment. In addition, the PL intensity and particle size of AIE-Tat-PMANPs did not show obvious variation during storage for 30 days, displaying good storage stability (Fig. 5D).

In summary, the AIE-Tat-PMANPs displayed a good fluorescence and colloidal stability against continuous UV light irradiation and pH variation of medium, as well as good storage stability. All these attributes were beneficial to biomedical applications, like cell fluorescence imaging.

Cytotoxicity and cell fluorescence imaging of AIE PMMA NPs, AIE-10%NH_2-PMANPs, and AIE-Tat-PMANPs

The cytotoxicity of various AIE NPs to HeLa cells after incubation for 24 h was investigated by MTT assay. As shown in Fig. 6A, the HeLa cells exhibited a cell viability more than 95% in the concentration range of 0–8 μg mL^{-1} of the AIE PMMA NPs and AIE-10%NH_2-PMANPs, displaying a low cytotoxicity. In comparison, the cell viability of HeLa cells slightly decreased to 82% with the increase of AIE-Tat-PMANP concentration from 0 to 8 μg mL^{-1}. The slightly reduced cell viability could be ascribed to the increased uptake efficiency of AIE-Tat-PMANPs by HeLa cells as a result of surface modification of HIV-1 Tat peptides. All the results showed that three types of NPs had low cytotoxicity in the experimental concentration range.

To ensure the good viability of cells, the NP concentration for the cell incubation prior to the cell fluorescence imaging was set at 4 μg mL^{-1}. The uptake ability of AIE-PNPs by HeLa cells was characterized by confocal laser microscopy, and the results are shown in Fig. 6B and C. As shown in Fig. 6B, the mean fluorescence signal intensity of HeLa cells incubated with various types of NPs generally increased with the incubation time, indicative of a continuous uptake process of

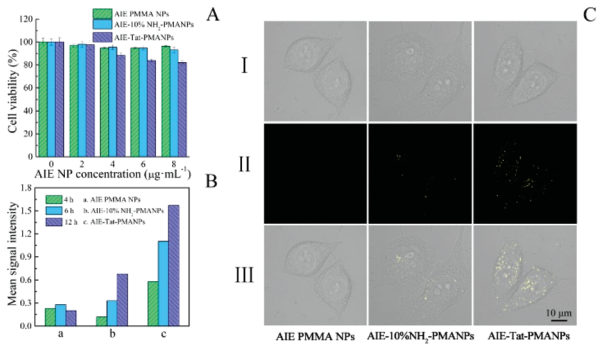

Fig. 6 (A) Cytotoxicity of the AIE PMMA NPs, AIE-10%NH_2-MANPs, and AIE-Tat-MANPs at various concentrations applied to HeLa cells after incubation for 24 h. (B) Time-dependent measurement of cellular uptake profiles in HeLa cells treated with AIE PMMA NPs, AIE-10%NH_2-MANPs, and AIE-Tat-MANPs, respectively. (C) CLSM images of HeLa cells after incubation with AIE PMMA NPs, AIE-10%NH_2-MANPs, and AIE-Tat-MANPs, respectively, for 12 h at 37 °C in bright field, fluorescence channel excited by 488 nm laser and emission within the range of 420–720 nm, and merged images. All the images share the same scale bar of 10 μm.

AIE-PNPs by cells. Moreover, the HeLa cells incubated with the AIE-Tat-PMANPs displayed 2.7 and 1.4 folds of mean fluorescence signal intensity after 12 h incubation, compared with the AIE PMMA NPs and AIE-10%NH_2-PMANPs, respectively (Fig. 6B). It demonstrated that the surface modification of HIV-1 Tat peptides significantly improved the uptake efficiency of AIE-PNPs by HeLa cells.

The incubated HeLa cells did not show an obvious morphology variation (Fig. 6C). The cells stained with the AIE PMMA NPs were hardly seen in the fluorescence channel, indicative of a low uptake amount of NPs by cells. The cells stained with the AIE-10%NH_2-PMANPs only showed weak yellow fluorescence (Fig. 6C). Promisingly, bright yellow fluorescence within the cytoplasm could be well observed in HeLa cells incubated with the AIE-Tat-PMANPs, which could be again ascribed to the high uptake efficiency of AIE-Tat-PMANPs by cells. Taking advantage of the surface modification of HIV Tat peptides, the cells could be well stained by the AIE-Tat-PMANPs at a lower NP concentration, compared with the reported results.[17,44]

Conclusion

Amino-functionalized AIE PNPs were efficiently synthesized through miniemulsion copolymerization of MMA and AEMH by using TPE-TCF as the AIEgen. The surface amino density of AIE-NH_2-MANPs could be conveniently tuned by the AEMH content. The surface amino groups served as the conjugation sites for the following maleimide and HIV-1 Tat peptide functionalization through the carbodiimide reaction and thiol-maleimide click reaction in sequential. The successful surface modification of AIE-NH_2-PMANPs was confirmed by the FTIR, ^1H NMR, and zeta-potential results. The AIE-Tat-PMANPs dis-

played good photostability under continuous UV irradiation, good photostability and colloidal stability under various pH values, as well as good storage stability. All these excellent attributes could be ascribed to the encapsulation of TPE-TCF by the polymer matrix. In comparison with the AIE PMMA NPs and AIE-10%NH_2-PMANPs, the AIE-Tat-PMANPs exhibited much better uptake efficiency and cell imaging quality at a relatively low NP concentration. So far, in our series of work,[17,24,25] we have completed the efficient synthesis of AIE-PNPs, precise brightness regulation, delicate surface modification with bioactive groups, and cell fluorescence imaging application. Our proposed miniemulsion-based technique may be widely used for efficient synthesis of AIE PNPs with versatile colors and sophisticated surface functionalization for bio-application.

Conflicts of interest

The authors declare no conflict of interest.

Acknowledgements

Financial support from the National Natural Science Foundation of China (NNSFC) project (51573168 and 21788102), the Science Foundation of Zhejiang Sci-Tech University (14012208-Y), the Excellent Young Researchers Foundation (CETT2015001) of Zhejiang Provincial Top Key Academic Discipline of Chemical Engineering and Technology, and National Undergraduate Training Programs for Innovation and Entrepreneurship of China (201710338021) is gratefully acknowledged.

References

1 Q. Y. Li, Y. H. Wu, H. Lu, X. Wu, S. Chen, N. Song, Y. W. Yang and H. Gao, *ACS Appl. Mater. Interfaces*, 2017, **9**, 10180–10189.
2 Z. F. Zhu, J. Qian, X. Y. Zhao, W. Qin, R. R. Hu, H. Q. Zhang, D. Y. Li, Z. P. Xu, B. Z. Tang and S. L. He, *ACS Nano*, 2016, **10**, 588–597.
3 H. Q. Peng, B. Liu, P. Wei, P. F. Zhang, H. K. Zhang, J. F. Zhang, K. Li, Y. Li, Y. H. Cheng, J. W. Y. Lam, W. J. Zhang, C.-S. Lee and B. Z. Tang, *ACS Nano*, 2019, **12**, 839–846.
4 G. W. Lin, P. N. Manghnani, D. Mao, C. Teh, Y. H. Li, Z. J. Zhao, B. Liu and B. Z. Tang, *Adv. Funct. Mater.*, 2017, **27**, 1701418.
5 D. Ding, K. Li, B. Liu and B. Z. Tang, *Acc. Chem. Res.*, 2013, **46**, 2441–2453.
6 G. X. Feng, R. T. K. Kwok, B. Z. Tang and B. Liu, *Appl. Phys. Rev.*, 2017, **4**, 021307.
7 A. Reisch and A. S. Klymchenko, *Small*, 2016, **12**, 1968–1992.
8 S. T. Selvan, T. T. Y. Tan, D. K. Yi and N. R. Jana, *Langmuir*, 2010, **26**, 11631–11641.
9 X. Wang, Y. Y. Yang, Y. P. Zhuang, P. Y. Gao, F. Yang, H. Shen, H. X. Guo and D. C. Wu, *Biomacromolecules*, 2016, **17**, 2920–2929.
10 Y. Guan, H. G. Lu, W. Li, Y. D. Zheng, Z. Jiang, J. L. Zou and H. Gao, *ACS Appl. Mater. Interfaces*, 2017, **9**, 26731–26739.
11 X. Y. Zhang, K. Wang, M. Y. Liu, L. Tao, Y. W. Chen and Y. Wei, *Nanoscale*, 2015, **7**, 11486–11508.
12 J. L. Yan, C. Estévez, J. E. Smith, K. M. Wang, X. X. He, L. Wang and W. H. Tan, *Nano Today*, 2007, **2**, 44–50.
13 Y. N. Hong, J. W. Y. Lam and B. Z. Tang, *Chem. Soc. Rev.*, 2011, **40**, 5361–5388.
14 J. Mei, Y. N. Hong, J. W. Y. Lam, A. J. Qin, Y. H. Tang and B. Z. Tang, *Adv. Mater.*, 2014, **26**, 5429–5479.
15 B. Z. Tang, X. W. Zhan, G. Yu, P. P. S. Lee, Y. Q. Liu and D. B. Zhu, *J. Mater. Chem.*, 2001, **11**, 2974–2978.
16 J. D. Luo, Z. L. Xie, J. W. Y. Lam, L. Cheng, H. Y. Chen, C. F. Qiu, H. S. Kwok, X. W. Zhan, Y. Q. Liu, D. B. Zhu and B. Z. Tang, *Chem. Commun.*, 2001, 1740–1741.
17 Z. H. Cao, X. Q. Liang, H. N. Chen, M. Gao, Z. J. Zhao, X. L. Chen, C. Xu, G. Qu, D. M. Qi and B. Z. Tang, *Polym. Chem.*, 2016, **7**, 5571–5578.
18 D. Ding, C. C. Goh, G. X. Feng, Z. J. Zhao, J. Liu, R. R. Liu, N. Tomczak, J. L. Geng, B. Z. Tang, L. G. Ng and B. Liu, *Adv. Mater.*, 2013, **25**, 6083–6088.
19 X. Hui, D. Z. Xu, K. Wang, W. J. Yu, H. Y. Yuan, M. Y. Liu, Z. Y. Shen, X. Y. Zhang and Y. Wei, *RSC Adv.*, 2015, **5**, 107355–107359.
20 H. Y. Li, X. Q. Zhang, X. Q. Zhang, K. Wang, H. L. Liu and Y. Wei, *ACS Appl. Mater. Interfaces*, 2015, **7**, 4241–4246.
21 M. W. Wang, N. Yang, Z. Q. Guo, K. Z. Gu, A. D. Shao, W. H. Zhu, Y. S. Xu, J. Wang, R. K. Prud'homme and X. H. Guo, *Ind. Eng. Chem. Res.*, 2015, **54**, 4683–4688.
22 J. Q. Xue, W. Bai, H. Y. Duan, J. J. Nie, B. Y. Du, J. Z. Sun and B. Z. Tang, *Macromolecules*, 2018, **51**, 5762–5772.
23 X. Y. Zhang, X. Q. Zhang, B. Yang, M. Y. Liu, W. Y. Liu, Y. W. Chen and Y. Wei, *Polym. Chem.*, 2014, **5**, 399–404.
24 X. Q. Liang, Y. X. Hu, Z. H. Cao, L. S. Xiao, J. J. Lou, L. Liu, Y. J. Wang, Z. J. Zhao, D. M. Qi and Q. M. Cui, *Dyes Pigm.*, 2019, **163**, 371–380.
25 Z. H. Cao, C. Xu, L. H. Liang, Z. J. Zhao, B. Chen, Z. J. Chen, H. N. Chen, G. Qu, D. M. Qi, G. R. Shan and U. Ziener, *Polym. Chem.*, 2015, **6**, 6378–6385.
26 F. J. Schork, Y. W. Luo, W. Smulders, J. P. Russum, A. Butté and K. Fontenot, *Adv. Polym. Sci.*, 2005, **175**, 129–255.
27 K. Landfester, *Angew. Chem., Int. Ed.*, 2009, **48**, 4488–4507.
28 D. M. Qi, Z. H. Cao and U. Ziener, *Adv. Colloid Interface Sci.*, 2014, **211**, 47–62.
29 J. M. Asua, *Prog. Polym. Sci.*, 2002, **27**, 1283–1346.
30 V. Holzapfel, A. Musyanovych, K. Landfester, M. R. Lorenz and V. Mailaender, *Macromol. Chem. Phys.*, 2005, **206**, 2440–2449.
31 J. Chen, P. S. Zhang, G. Fang, P. G. Yi, X. Y. Yu, X. F. Li, F. Zeng and S. Z. Wu, *J. Phys. Chem. B*, 2011, **115**, 3354–3362.

32 Y. J. Wang, Y. Shi, Z. Y. Wang, Z. F. Zhu, X. Y. Zhao, H. Nie, J. Qian, A. J. Qin, J. Z. Sun and B. Z. Tang, *Chem. – Eur. J.*, 2016, **22**, 9784–9791.
33 M. S. Muthu, R. V. Kutty, Z. T. Luo, J. P. Xie and S.-S. Feng, *Biomaterials*, 2015, **39**, 234–248.
34 T. Delair, V. Marguet, C. Pichot and B. Mandrand, *Colloid Polym. Sci.*, 1994, **272**, 962–970.
35 D. M. Copolovici, K. Langel, E. Eriste and Ü. Langel, *ACS Nano*, 2014, **8**, 1972–1994.
36 X. T. Ji, R. Y. Zhang, Z. B. Wang, S. Y. Niu and C. F. Ding, *ACS Appl. Bio Mater.*, 2018, **2**, 370–377.
37 W. B. Wu, D. Mao, F. Hu, S. D. Xu, C. Chen, C.-J. Zhang, X. M. Cheng, Y. Y. Yuan, D. Ding, D. L. Kong and B. Liu, *Adv. Mater.*, 2017, **29**, 1700548.
38 X. Zhang, G. G. Sun, M. Hovestädt, V. Syritski, N. Esser, R. Volkmer, S. Janietz, J. Rappich and K. Hinrichs, *Electrochem. Commun.*, 2010, **12**, 1403–1406.
39 D. Pranantyo, L. Q. Xu, E.-T. Kang and M. B. Chan-Park, *Biomacromolecules*, 2018, **19**, 2156–2165.
40 L. Hyndman, J. L. Lemoine, L. Huang, D. J. Porteous, A. C. Boyd and X. Nan, *J. Controlled Release*, 2004, **99**, 435–444.
41 D. Wang, J. Qian, W. Qin, A. J. Qin, B. Z. Tang and S. L. He, *Sci. Rep.*, 2014, **4**, 4279.
42 J. Y. Xiang, X. L. Cai, X. D. Lou, G. X. Feng, X. H. Min, W. W. Luo, B. R. He, C. C. Goh, L. G. Ng, J. Zhou, Z. J. Zhao, B. Liu and B. Z. Tang, *ACS Appl. Mater. Interfaces*, 2015, **7**, 14965–14974.
43 W. H. Zhuang, Y. Y. Xu, G. C. Li, J. Hu, B. X. Ma, T. Yu, X. Su and Y. B. Wang, *ACS Appl. Mater. Interfaces*, 2018, **10**, 18489–18498.
44 H. Y. Li, X. Q. Zhang, X. Y. Zhang, B. Yang, Y. Yang and Y. Wei, *Polym. Chem.*, 2014, **5**, 3758–3762.